CrystEngComm

Temperature-induced racemic compounds and chiral conglomerates based on polyoxometalates and lanthanides: syntheses, structures and catalytic properties

Journal:	*CrystEngComm*
Manuscript ID:	CE-ART-09-2014-001802.R1
Article Type:	Paper
Date Submitted by the Author:	02-Oct-2014
Complete List of Authors:	An, Haiyan; College of Chemistry, Dalian University of Technology, Wang, Lin; College of Chemistry, Dalian University of Technology, Hu, Ying; College of Chemistry, Dalian University of Technology, Fei, Fei; College of Chemistry, Dalian University of Technology,

Temperature-induced racemic compounds and chiral conglomerates based on polyoxometalates and lanthanides: syntheses, structures and catalytic properties

Haiyan An,* Lin Wang, Ying Hu, Fei Fei

College of Chemistry, Dalian University of Technology, Dalian 116023, P. R. China

*Corresponding author. Tel: +86-411-84657675. E-mail address: anhy@dlut.edu.cn

Abstract

By controlling the reaction temperatures, four new architectures based on Evans-Showell type polyoxometalate, $[Ln(H_2O)_5][Ln(H_2O)_7][Co_2Mo_{10}H_4O_{38}]$ $6H_2O$ (Ln = Sm **1**; Eu **2**), and $(NH_4)_3[Ln(H_2O)_6][Co_2Mo_{10}H_4O_{38}]$ $6H_2O$ (Ln = Sm **3**; Eu **4**) have been synthesized and characterized by elemental analysis, IR spectroscopy, TG analysis, solid diffuse reflective spectrum, powder X-ray diffraction and single crystal X-ray diffraction. Compounds **1** and **2** are racemic compounds, obtained at the higher temperature (85 ^oC). They show a 1D ladderlike structure constructed from left-handed chain and right-handed chain linked by lanthanide cations, which represent the first 1D self assembly based on Evans-Showell type polyoxometalate. When the reaction temperature was decreased to room temperature (25 ^oC), two chiral species **3** and **4** were got, showing a mono-supporting structure composed of one $[Co_2Mo_{10}H_4O_{38}]^{6-}$ polyoxoanion and one $[Ln(H_2O)_6]^{3+}$ unit. They crystallize in the chiral space group $P2_1$, as conglomerates of two enantiomerically pure crystals. Their absolute configuration were determined by the Flack parameters and solid state circular dichroism spectroscopy. The structural differences between **1**(**2**) and **3**(**4**) reveal the reaction temperature is the key factor controlling the products from racemic compounds to conglomerates. Four compounds **1–4** acted as Lewis acid−base catalysts through a heterogeneous manner to prompt cyanosilylation with excellent efficiency.

Introduction

The construction of chiral polyoxometalates (POMs) is a topical area owing to their intriguing variety of architectures and topologies, as well as potential applications in catalysis, nonlinear optics, medicine.[1] In recent years, thanks to the prominent work of Pope, Hill, Yamase, Kortz, Cronin, Wang, Su, Wei and Hasenknopf, a few chiral compounds based on POMs have been prepared.[2-6] Usually, these chiral POM-based compounds can be synthesized using chiral inducement, including chiral organic ligands and chiral metal-organic compounds.[7-9] Spontaneous resolution from achiral materials is the other interesting, but challenging method to prepare chiral POMs.[10] Statistically, only 5−10% of all racemates can form conglomerate crystals (in which molecules form condensates comprising only one enantiomer, but the sample as a whole is racemic), indicating the difficulty to realize spontaneous resolution.[11] Hill's group documented the first spontaneous resolution of chiral POMs. Two enantiomerically pure chiral hafnium-substituted polyoxometalates $[Hf(PW_{11}O_{39})_2]^{10-}$ were synthesized in the absence of any chiral source upon crystallization.[12] Wei and co-workers successfully discovered two interesting examples of chiral POMs formed by spontaneous resolution:[13] one is by assembling achiral Lindqvist and Anderson anions into a triad via organic ligands with rotatable covalent bonds; the other is a novel POM-based chiral macrocycle from the achiral Lindqvist hexamolybdate and bisarylamines. Wang et al. used the classical Waugh-type polyoxoanion $[MnMo_9O_{32}]^{6-}$ as a model, and changed the racemic $[MnMo_9O_{32}]^{6-}$ from a racemic compound via a racemic solid solution to a conglomerate by adjusting the linkers

from imidazole molecules to Na^+ and finally transition-metal cations.[14] Although some groups have made great contributions to construct chiral POMs by spontaneous resolution, the information on the factors which mediate the formation of conglomerates vs racemic compounds has been little known up to now. Therefore, it is still a formidable challenge to build POM-based conglomerates and racemic compounds and look for the factors that control their formation.

To meet such a challenge, we choose the reaction system of Evans-Showell type $[Co_2Mo_{10}H_4O_{38}]^{6-}$ anion as subunit and lanthanides as linker, because: (i) the $[Co_2Mo_{10}H_4O_{38}]^{6-}$ anion possesses a point group symmetry D_2 which will induce the formation of chiral species, similar to $[MnMo_9O_{32}]^{6-}$ polyoxoanion with a D_3 symmetry;[15] (ii) no information on structure and property has been reported in using $[Co_2Mo_{10}H_4O_{38}]^{6-}$ as building block for the fabrication of extended frameworks since its structure was solved at 1969; (iii) there are two terminal oxygen atoms on each molybdenum center of $[Co_2Mo_{10}H_4O_{38}]^{6-}$ anion which make it have strong coordination ability to lanthanides to form new inorganic architectures. We herein expect that the $[Co_2Mo_{10}H_4O_{38}]^{6-}$ anion should be a suitable building unit utilized in constructing chiral POMs through controlling the reaction conditions.

It is well-known that many external factors, such as pH values, solvent systems, and metal-to-POM ratios impose crucial influences on the structures of compounds, although it remains a considerable difficulty to control the structures of POM-based materials. Most research results suggest that a subtle alteration by means of these factors can lead to totally different products.[16-18] However, one factor, reaction

temperature is often ignored to target this kind of goal. So far, there are very limited examples of temperature-controlled self assembly of non-chiral POMs. For instance, Niu and coworkers reported three new inorganic–organic hybrid arsenomolybdates originated from different temperature ranges corresponding to different proportions of oxidized AsIII atoms;[19] Cronin's group successfully isolated two 3D open framework materials using a preassembled anion $\{P_8W_{48}\}$, and electrophilic manganese Mn^{2+} linkers by the temperature control;[20] Dessapt et al. studied the reactivity of MoO_4^{2-} toward six organoammonium cations at different synthesis temperatures, and got 16 organic-inorganic hybrid materials.[21] It is thus of considerable interest to investigate whether reaction temperature can play a vital factor to impact the formation of chiral POMs.

In this work, we study the interactions between the Evans-Showell type cluster $[Co_2Mo_{10}H_4O_{38}]^{6-}$ and lanthanide cations at different temperatures. Four new compounds were obtained, namely $[Ln(H_2O)_5][Ln(H_2O)_7][Co_2Mo_{10}H_4O_{38}]\cdot 6H_2O$ (Ln = Sm **1**; Eu **2**), and $(NH_4)_3[Ln(H_2O)_6][Co_2Mo_{10}H_4O_{38}]\cdot 6H_2O$ (Ln = Sm **3**; Eu **4**). Compounds **1** and **2** obtained at 85^{o}C are constructed from left-handed chain and right-handed chain to form a 1D racemic ladder, representing the first examples of 1D extended structures based on the Evans-Showell type polyoxoanion. Compounds **3** and **4** got at 25^{o}C are chiral conglomerates, which crystallize in the chiral space group $P2_1$. All four compounds as Lewis acid−base catalysts are very efficient in the cyanosilylation of carbonyl compounds and allow the reaction to be carried out under solvent-free conditions using only a low loading of the catalyst, which can be

recovered and reused without displaying any significant loss of activity.

Experimental section

Materials and measurements

All chemicals were commercially purchased and used without further purification. The metal chlorides $LnCl_3$ (Ln= Sm, Eu) were prepared by dissolving Ln_2O_3 (99.9%) in hydrochloric acid, followed by drying and crystallization. $(NH_4)_6[Co_2Mo_{10}H_4O_{38}]\cdot 7H_2O$ was synthesized according to the literature,[22,15] and characterized by means of IR spectroscopy. Elemental analyses (H and N) were performed on a Perkin-Elmer 2400 CHN elemental analyzer; Co, Mo, Sm and Eu were analyzed on a PLASMA-SPEC (I) ICP atomic emission spectrometer. IR spectra were recorded in the range 400–4000 cm^{-1} on an Alpha Centaur FT/IR Spectrophotometer using KBr pellets. TG analyses were performed on a Perkin-Elmer TGA7 instrument in flowing N_2 with a heating rate of 10 ºC·min^{-1}. PXRD patterns of the samples were recorded on a Rigaku Dmax 2000 X-ray diffractometer with graphite monochromatized Cu−Kα radiation (λ = 0.154 nm) and 2θ varying from 5 to 50°. Diffuse reflectivity spectra were collected on a finely ground sample with a Cary 500 spectrophotometer equipped with a 110 mm diameter integrating sphere, which were measured from 200 to 800 nm. CD spectra were measured on JASCO J-810.

Synthesis of $[Sm(H_2O)_5][Sm(H_2O)_7][Co_2Mo_{10}H_4O_{38}]\cdot 6H_2O$ (1)

In a typical synthesis procedure for **1**, $SmCl_3$ (0.015 g, 0.06 mmol) and $(NH_4)_6[Co_2Mo_{10}H_4O_{38}]\cdot 7H_2O$ (0.058 g, 0.03 mmol) were dissolved in 10 mL water. Then 10 mL acetonitrile was added to the above solution. The pH value of the mixture

was about 3.00. The mixture was heated at 85 °C for 20 h and dark green plate-shaped crystals of **1** were collected in about 30% yield (based on Mo). Elemental analyses: Calc. for **1**: H, 1.73; Co, 5.09; Mo, 41.46; Sm, 12.99%. Found H, 1.81 Co, 5.34; Mo, 41.20; Sm, 13.26%. FTIR data (cm^{-1}): 3432(s), 1631(m), 943(vs), 921(vs), 854(m), 633(vs), 596(vs), 559(s), 453(m).

Synthesis of $[Eu(H_2O)_5][Eu(H_2O)_7][Co_2Mo_{10}H_4O_{38}]\cdot 6H_2O$ (2)

The preparation of **2** was similar to that of **1** except that $EuCl_3$ (0.015g, 0.06mmol) was used instead of $SmCl_3$. The pH value of the mixture was about 3.05. Dark green plate-shaped crystals of compound **2** were obtained in about 20% yield (based on Mo). Elemental analyses: Calc. for **2**: H, 1.73; Co, 5.09; Mo, 41.40; Eu, 13.11. Found H, 1.89; Co, 5.33; Mo, 41.27; Eu, 13.35%. FTIR data (cm^{-1}): 3396(s), 1626(m), 952(vs), 914(vs), 631(vs), 600(vs), 572(s), 445(m).

Synthesis of $(NH_4)_3[Sm(H_2O)_6][Co_2Mo_{10}H_4O_{38}]\cdot 6H_2O$ (3)

In a typical synthesis procedure for **3**, $SmCl_3$ (0.015 g, 0.06 mmol) and $(NH_4)_6[Co_2Mo_{10}H_4O_{38}]\cdot 7H_2O$ (0.058 g, 0.03 mmol) were dissolved in 10 mL water. Then 10 mL acetonitrile was added to the above solution. The pH value of the mixture was about 3.00. The mixture was kept at room temperature for several days, and then dark green block crystals of **3** were collected in about 40% yield (based on Mo). Elemental analyses: Calc. for **3**: H, 1.90; N, 1.99; Co, 5.59; Mo, 45.47; Sm, 7.13%. Found: H, 2.11; N, 2.24; Co, 5.34; Mo, 45.62; Sm, 6.97%. FTIR data (cm^{-1}): 3436(s) 1632(m), 1404(m), 952(vs), 917(vs), 854(m), 631(vs), 596(vs), 547(s), 445(w).

Synthesis of $(NH_4)_3[Eu(H_2O)_6][Co_2Mo_{10}H_4O_{38}]\cdot 6H_2O$ (4)

The preparation of **4** was similar to that of **3** except that $EuCl_3$ (0.015g, 0.06mmol) was used instead of $SmCl_3$. The pH value of the mixture was about 3.05. Dark green block crystals of compound **4** were obtained in about 35% yield (based on Mo). Elemental analyses: Calc. for **4**: H, 1.89; N, 1.99; Co, 5.58; Mo, 45.44; Eu, 7.20%. Found: H, 2.13; N, 1.87; Co, 5.73; Mo, 45.29; Eu, 7.41%. FTIR data (cm^{-1}): 3433(m), 1633(m), 1403(s), 948(vs), 915(vs), 854(m), 632(vs), 600(vs), 547(s), 449(w).

X-Ray crystallography

The crystallographic data of four compounds were collected on the Bruker Smart CCD diffractometer with Mo Kα radiation (λ=0.71073 Å) by ω and θ scan modes at 293K for **1** and at 296 K for **2–4**. Empirical absorption correction was applied. The structures of **1–4** were solved by the direct method and refined by the Full-matrix least squares on F^2 using the SHELXTL-97 software.[23] All of the non-hydrogen atoms were refined anisotropically in **1–4**. The hydrogen atoms attached to oxygen atoms of polyoxoanions and water molecules were not located in **1–4**. Site occupancies of the partial crystal water molecules and/or partial free ammonium molecules in **1–4** were set to be less than 1 through the refinement of their thermal parameters due to disorder. Other restraints such as 'isor' were used in the refinements for obtaining reasonable atom sites and thermal parameters. A summary of the crystallographic data and structural determination for **1–4** is provided in Table 1.

CSD reference number: 428383, 428384, 428385, 428386 for **1–4**.

General procedure for cyanosilylation reactions

A typical procedure for the cyanosilylation reaction of aldehydes is as follows: 2 mol % catalyst (**1**–**4**) was added to a mixture of aldehyde (0.5 mmol) and $(CH_3)_3SiCN$ (1.5 mmol), in the absence of solvent. The reaction mixture was stirred at room temperature under a N_2 atmosphere. The progress of the reaction was monitored by GC analysis. After the reaction was completed, the catalyst was removed by filtration and centrifugation of the reaction mixture. All products (cyanohydrin trimethylsilyl ethers) were confirmed by a comparison of their GC retention times, GC-MS spectra, and/or ^1H spectra with those of authentic data. GC analysis was performed using HP6890/5973MS with a cross-linked (95%)-dimethyl-(5%)-diphenylpolysiloxane column of 30 m length.

Results and Discussion

Synthesis

The reaction of $(NH_4)_6[Co_2Mo_{10}H_4O_{38}]\cdot 7H_2O$ and $LnCl_3$ (Ln = Sm, Eu) has been investigated. Four compounds with two kinds of structures were obtained. Compounds **1**(**2**) and **3**(**4**) were synthesized under the same reaction conditions, except for the alternation of reaction temperature. It is clear that the reaction temperature of the reaction system is the key factor influencing the structures and topologies of these compounds. At higher temperature (85^oC), racemic compounds **1** and **2** $[Ln(H_2O)_5][Ln(H_2O)_7][Co_2Mo_{10}H_4O_{38}]$ are isolated, exhibiting a 1D ladderlike frame; with a decrease of the temperature to room temperature (25^oC), 0D mono-supporting chiral architectures **3** and **4** $(NH_4)_3[Ln(H_2O)_6][Co_2Mo_{10}H_4O_{38}]$ are formed by chiral resolution of Evans-Showell type POM with lanthanides. The

increasing temperature makes the solution reaction more effective, so more lanthanide cations substitute NH_4^+ to coordinate to the terminal oxygen atoms of polyoxoanions to produce extended structures. Then, we can assume that compounds **3** and **4** are the kinetic phase because they are formed at milder conditions. On the other hand, compounds **1** and **2** seem to be the thermodynamic phase. To our best knowledge, compounds **1**(**2**) and **3**(**4**) represent the first example of temperature-controlled structural changes from racemic compounds to chiral conglomerates in the field of POMs.

When Gd^{3+} or Tb^{3+} ion with smaller ionic radii was used instead of Sm^{3+} or Eu^{3+} ion, at room temperature (25^{o}C) two chiral compounds that are isostructrural to compounds **3** and **4** were also got, while at higher temperature (85^{o}C), two racemic high-dimensional structures in which partial Gd^{3+} and Tb^{3+} ions are eight-coordinate geometry were separated. The experimental results further indicate that the reaction temperature is the key factor mediating the formation of chiral conglomerates *vs* racemic compounds in the reaction system of Evans-Showell type POM, as well as the solid-state structures adopted by these compounds are imposed by the nature of the lanthanide cations used.

Many parallel experiments indicate that stoichiometry and pH value also can affect the quality of crystals. The products are obviously affected by the stoichiometry of $Ln^{3+}/[Co_2Mo_{10}H_4O_{38}]^{6-}$. Compounds **1–4** can be well isolated by the 2:1 $Ln^{3+}/[Co_2Mo_{10}H_4O_{38}]^{6-}$ ratio. When the $Ln^{3+}/[Co_2Mo_{10}H_4O_{38}]^{6-}$ ratio increased from 2:1 to 3:1 or 4:1, the crystal quality of compounds **1–4** was poor, and the yields were

reduced. The optimal pH range of the reaction is from 2.0 to 4.0. For a low pH (pH<2.0) no reaction occurs; for a high pH (pH > 4.0) the hydrolysis of the lanthanide cations makes a mass of precipitates. This is consistent with the stable pH range of Evans-Showell type cluster $[Co_2Mo_{10}H_4O_{38}]^{6-}$.[24]

Crystal structures of 1 and 2

Single-crystal X-ray crystallographic analyses reveal that the heteropolymolybdate $[Co_2Mo_{10}H_4O_{38}]^{6-}$ in compounds **1–4** is a typical Evans-Showell type polyoxoanion. The polyoxoanion $[Co_2Mo_{10}H_4O_{38}]^{6-}$ was first prepared by Friedheim and Keller in 1906,[25] and was structurally determined as its ammonium salt by Evans and Showell in 1969.[15] The structure of $[Co_2Mo_{10}H_4O_{38}]^{6-}$ can be deduced from the planar Anderson ion $[CoMo_6H_6O_{24}]^{3-}$ by removing one $\{MoO_5\}$ group from each of two $[CoMo_6H_6O_{24}]^{3-}$ ions, turning one ~45° around the anionic equatorial plane and joining them so that the two CoO_6 octahedra share an edge. As suggested by Evans and Showell, the polyoxoanion $[Co_2Mo_{10}H_4O_{38}]^{6-}$ has a point group symmetry D_2, and possesses two enantiomers (shown in Scheme 1).

Isostructural compounds **1** and **2** crystallize in the centrosymmetric space group *P*-1, thus two enantiomers of the polyoxoanion can coexist in the crystal lattice. Herein compound **1** is described as an example in detail. The structure of **1** exhibits a unique 1D ladderlike chain assembled by $[Co_2Mo_{10}H_4O_{38}]^{6-}$ polyoxoanions and Sm^{3+} cations. In the asymmetric unit, one crystallization-independent $[Co_2Mo_{10}H_4O_{38}]^{6-}$ anion is linked by two unique Sm^{3+} cations (Fig. 1a). In the polyoxoanion, four of the 10 crystallographically unique oxygen atoms surrounding the two Co^{3+} ions, are

bound to hydrogen atoms, which are identified by the calculation of bond valence sums. Six kinds of oxygen atoms exist in the cluster according to the manner of oxygen coordination, that is terminal oxygen Ot, terminal oxygen Ot' linked to Sm^{3+}, double-bridging oxygen Ob, central oxygen Oc (μ_3-OH atom of a Co and two Mo atoms), central oxygen Od (μ_4-O atom of a Co and three Mo atoms), central oxygen Oq (μ_4-O atom of two Co and two Mo atoms). Thus the Mo–O bond lengths fall into six classes: Mo–Ot 1.681(6)–1.725(6) Å, Mo–Ot' 1.713(6)–1.728(6) Å, Mo–Ob 1.874(6)–1.972(6) Å, Mo–Oc 2.229(5)–2.288(6) Å, Mo–Od 1.989(5)–2.363(5) Å and Mo–Oq 2.222(5)–2.333(5) Å in **1**. The central Co–O distances are 1.871(5)–1.958(5) Å, and the O-Co-O angles are in the range of 83.5(2)–175.8(2)°. All bond lengths and bond angles are within the normal ranges.[15,22]

The two crystallization-independent Sm(III) cations display a similar coordination sphere (Fig. S1). Sm(1) cation, joined neighboring $[Co_2Mo_{10}H_4O_{38}]^{6-}$ polyoxoanions together as linker, has a tricapped trigonal prism coordination environment, defined by four terminal oxygen atoms from two $[Co_2Mo_{10}H_4O_{38}]^{6-}$ units [Sm–O 2.448(5)–2.628(6) Å] and five water molecules [Sm–OH_2 2.399(6)–2.557(8) Å]. The nine-coordinate Sm(2) links to two terminal oxygen atoms from two $[Co_2Mo_{10}H_4O_{38}]^{6-}$ molecules [Sm–O 2.483(6)–2.526(6) Å] and seven water molecules [Sm–OH_2 2.430(7)–2.539(8) Å] to complete a tricapped trigonal prism coordination geometry. The average Sm–O bond length is 2.480 Å.

Interestingly, in **1** homochiral $[Co_2Mo_{10}H_4O_{38}]^{6-}$ anions are linked by Sm(1) cations to generate a 1D chiral chain (Fig. 2a). Adjacent opposite-handed chiral chains are

interconnected by Sm(2) cations to produce a 1D non-chiral ladderlike structure along the *c* axis (shown in Fig. 2b). To our best knowledge, compounds **1** and **2** represent the first examples of 1D architectures based on $[Co_2Mo_{10}H_4O_{38}]^{6-}$ unit. Then adjacent non-chiral ladderlike chains are linked together by hydrogen-bonding interactions (O14···O1W 2.861, O9···O1W 2.866, O22···O2W 2.910 Å) between terminal oxygen atoms of polyoxoanions and coordinated water molecules to form an interesting 2D supramolecular network (see Fig. 3a). Furthermore, 2D supramolecular layers are joined up to yield a 3D supramolecular framework via other hydrogen-bonding interactions (O21···O4W 2.713, O25···O4W 2.904, O36···O6W 2.882, O12···O8W 2.858 Å) (see Fig. 3b). Free water molecules are filled in the cavities and participate in the extensive hydrogen-bonding interactions with the polyoxoanion framework.

Crystal structures of 3 and 4

The preparation of compounds **3** and **4** was similar to that of compounds **1** and **2** except that the reaction temperature was adjusted from 85 ^{o}C to room temperature (25^{o}C). Single crystal structural analysis revealed that compounds **3** and **4** are isostructural, and crystallize in the chiral space group $P2_1$ with Flack parameters of 0.025(8) (**3**) and 0.042(8) (**4**). Thus, compound **3** will be described. Compound **3** exhibits a mono-supporting structure assembled by chiral $[Co_2Mo_{10}H_4O_{38}]^{6-}$ polyoxoanion and one Sm^{3+} cation with three NH_4^+ balancing the charges. The structure of $[Co_2Mo_{10}H_4O_{38}]^{6-}$ anion is also an Evans-Showell type, similar to compound **1**. Six kinds of oxygen atoms exist in the cluster according to the manner of oxygen coordination. Then, the Mo–O bond lengths fall into six classes: Mo–Ot

1.682(5)–1.730(5) Å, Mo–Ot' 1.727(5)–1.740(5) Å, Mo–Ob 1.847(5)–1.987(5) Å, Mo–Oc 2.233(5)–2.287(5) Å, Mo–Od 1.980(5)–2.369(5) Å and Mo–Oq 2.210(5)–2.363(5) Å in **3**. The central Co–O distances are 1.857(4)–1.936(5) Å, and the O-Co-O angles are in the range of 83.8(2)–175.9(2)°. The asymmetric unit in the structure of **3** consists of one crystallographically independent chiral Evans-Showell type polyoxoanion linked by one Sm^{3+} unit (Fig. 1b). The crystallographically unique Sm^{3+} ion bonded to the polyoxoanion as supporter, is coordinated by three oxygen atoms from the POM [Sm–O 2.446(5)–2.491(5) Å] and six water molecules [Sm–OH_2 2.437(6)–2.523(6) Å] to form a monocapped square antiprismatic coordination geometry (Fig. S2). The average Sm–O bond length is 2.477 Å.

Remarkably, in **3** theses mono-supporting chiral subunits are firstly joined up together by the strong hydrogen-bonding interactions (O33···O2W 2.766 Å) between terminal oxygen atoms of polyoxoanions and coordinated water molecules to form a 1D supramolecular chiral chain (shown in Fig. 4a). Then adjacent homochiral chains are linked together by other hydrogen-bonding interactions (O30···O3W 2.892 Å) to generate an interesting 2D supramolecular wavelike network (see Fig. 4b). Furthermore, 2D supramolecular layers are connected to yield a 3D supramolecular chiral framework via the strong hydrogen-bonding interactions (O20···O6W 2.730 Å) (Fig. 5). Free water molecules and NH_4^+ ions are filled in the cavities of 3D supramolecular structures and participate in the extensive hydrogen-bonding interactions with the polyoxoanion framework. A better insight into the nature of such 3D supramolecular framework can be achieved by reducing the structure to simple

node and linker net. According to the simplification principle, each Sm(1) cation is linked with four $[Co_2Mo_{10}H_4O_{38}]^{6-}$ units, and the $[Co_2Mo_{10}H_4O_{38}]^{6-}$ unit is bonded to four adjacent Sm(1) cations through hydrogen bonds. Therefore, the resulting 3D supramolelar chiral frame is a uninodal 4-connected diamond-related net with Schläfli symbol of 6^6, as shown in Fig. S3.

Bond valence sum calculations[26] show that all Mo atoms are in the +6 oxidation state, Co atoms are in the +3 oxidation state, and lanthanide sites are in the +3 oxidation state. These results are consistent with the charge balance considerations.

FT-IR spectroscopy

IR spectra of compounds **1**–**4** display similar characteristic patterns of the Evans-Showell type structure $[Co_2Mo_{10}H_4O_{38}]^{6-}$ (see Fig. S4a-S4d), in agreement with those reported in literatures.[22] The spectra can be divided into the following typical regions: (1) 3600–2800 cm^{-1} corresponding to the O–H and N–H stretchings; (2) 1700–1400 cm^{-1} corresponding to the region of the O–H and N–H bendings; (3) 1000–850 cm^{-1} assignable to the Mo–O terminal stretchings; (4) 750–500 cm^{-1} assignable to the Mo–O–Mo bridge stretchings (the vibrations of the Mo–O–Co bonds and the water librations are also located in this last region). Below 500 cm^{-1}, the spectrum is rather difficult to analyze, the bending of the Mo–Ot and Mo–Ob bonds can be mixed with the Mo–Oc stretching vibrations. Notice that the IR spectra of **3** and **4** respectively show an additional vibration band at 1404 and 1403 cm^{-1} which is attributable to the N–H bending in the NH_4^+ cations, compared with those of **1** and **2**. These results are consistent with the single-crystal X-ray analyses.

TG analysis

Thermal gravimetric (TG) curve of **1** is shown in Fig. S5a. The TG curve exhibits a multi-step continuous weight loss process and gives a total weight loss of 16.1% in the range of 40–600 ºC, which agrees with the calculated value of 16.3%. The weight loss of 13.4% from 40 to 270 ºC corresponds to the loss of all lattice and coordinated water molecules (calc. 14.0%). The weight loss of 2.7% from 275 to 470 ^{o}C is due to the loss of composition water molecules and oxygen molecules from the residual metal oxides (calc. 2.3%). The TG curves of **2** exhibits similar weight loss stages to those of **1** (see Fig. S5b), and gives a total weight loss of 16.3% in the range of 40–600 ºC, which agrees with the calculated value of 16.2%.

Thermal gravimetric (TG) curve of **3** is shown in Fig. S5c. The TG curve exhibits a multi-step continuous weight loss process and gives a total weight loss of 15.5% in the range of 40–600 ºC, which agrees with the calculated value of 15.1%. The weight loss of 10.5% from 40 to 265 ºC corresponds to the loss of all lattice and coordinated water molecules (calc. 10.2%). The weight loss of 5.0% from 267 to 480 ^{o}C is due to the loss of composition water molecules, ammonia molecules, and oxygen molecules from the residual metal oxides. The TG curves of **4** exhibits similar weight loss stages to those of **3** (see Fig. S5d), and gives a total weight loss of 15.2% in the range of 40–600 ºC, which agrees with the calculated value of 15.1%.

PXRD characterization

The PXRD patterns for **1**–**4** are presented in Fig. S6. The diffraction peaks of both calculated and experimental patterns match well, indicating the phase purities of these

compounds. The differences of PXRD patterns of **1**(**2**) and **3**(**4)** also indicate that both kinds of compounds have different structures. These conclusions are in agreement with the results of the single crystal X-ray analysis.

UV-Vis diffuse reflective spectroscopy

The diffuse reflectivity for solid samples of **1**−**4** were performed. The absorption (*A*) data were calculated from the reflectivity using the function: $A = \log(1/R\%)$ where *R* is the reflectivity at a given wavelength (λ). The *A* versus λ plots are displayed in Fig. 6. On the UV region (200–400 nm), the plots display two intense absorption bands at 223, 304 nm for **1**, 227, 305 nm for **2**, 225, 303 nm for **3**, and 225, 303 nm for **4**, which are characteristic of O→Mo charge transfer for POMs. On the visible region (400–800 nm), there are also two absorption bands at 440, 605 nm for **1**, 442, 607 nm for **2**, 441, 605 nm for **3** and 441, 605 nm for **4**, which are respectively attributed to the $^1A_{1g} \rightarrow {}^1T_{2g}$ and $^1A_{1g} \rightarrow {}^1T_{1g}$ transition of a regular octahedral configuration low-spin Co^{3+} in the $[Co_2Mo_{10}H_4O_{38}]^{6-}$ anion.[27]

CD spectroscopy

One pair of enantiomers L-**3** and D-**3** were separated manually. The solid state CD spectra of the bulk samples of L-**3** and D-**3** are mirror images of each other, which indicated that both compounds are enantiomers (Fig. 7). In the λ = 200–400 nm wavelength range, L-**3** and D-**3** showed clearly cotton effects at about 252 nm and 316 nm. The two absorption bands can be assigned to the O→Mo LMCT transition for $[Co_2Mo_{10}H_4O_{38}]^{6-}$ anion.

Catalysis study

Cyanosilylation reaction provides a convenient route to cyanohydrins, which are key derivatives in the synthesis of fine chemicals and pharmaceuticals. In order to obtain cyanohydrin molecules, the use of a catalyst with Lewis acid or base character through which both the substrate and the cyanide precursor are activated is necessary.[28] In this sense, the starting substrates commonly used are aldehydes or ketones with trimethylsilyl cyanide (TMSCN) as the nucleophilic agent. In this work, we test the activity of four compounds **1**–**4** as a heterogeneous catalyst in the aldehyde cyanosylation reaction under solvent-free condition at room temperature.

Firstly, the cyanosilylation of benzaldehyde acts as a model reaction to investigate the catalytic nature of compounds **1**–**4**. The reaction was carried out with 2 mol % of catalysts under the conditions described in Table 2. All our compounds effectively catalyzed the cyanosilylation to afford the corresponding cyanohydrin trimethylsilyl ether with yield of up to about 98%. In a comparison of the reactivity of our catalysts with that of some previously reported POM-based compounds ($[Cu_2(bpy)(H_2O)_{5.5}]_2[H_2W_{11}O_{38}]$ and $TBA_8H_2[(SiYW_{10}O_{36})_2]$),[29] it was found to be higher than the first one (benzaldehyde, 24 h, and yield = 98.1%), which uses solvent conditions, and less than the second one, which is a homogeneous catalyst and uses solvent conditions (benzaldehyde, 15 min, and yield = 94%).

Subsequently, the cyanosilylation reaction of various kinds of aromatic aldehyde substrates in the presence of catalysts **1** and **3** was further studied. With a substrate like 2-hydroxybenzaldehyde, 4-methylbenzaldehyde, or 4-fluorobenzaldehyde, the yield is high (Table 2). It seems that the nature of the substituent on the aromatic ring

had no dramatic effect on the reaction yield. When sterically more hindered 1-napthaldehyde is used as the substrate, the yield is very poor suggesting that the aldehyde here is not accommodated as per the transition-state geometry requirement for driving the reaction to the product according to the Lewis acid effect of lanthanides. [30]

To probe the heterogeneity of the catalysts, after the catalytic reactions, the catalysts were recovered from their reaction media. Solids of **1** and **3** could be easily isolated from the reaction suspension by a simple filtration and reused at least three times without an appreciable loss of its high catalytic performance (from 98.2% to 96.9% yield; from 98.4% to 96.4% yield see Table S2). The PXRD patterns of the retrieved catalysts were identical with those of the fresh catalysts (Fig. S7). The IR spectra of the recovered compounds **1** and **3** were also identical to those of the freshly prepared samples (Fig. S8). These observations suggested that **1** and **3** are true heterogeneous catalysts. In addition, infrared spectroscopy of the catalysts **1** and **3** impregnated with benzaldehyde exhibited one broad C−O stretch at 1689.6 and 1691.0 cm^{-1}, respectively. The ν(C−O) stretch had a red shift of ~12.2 and 10.8 cm^{-1} from 1701.8 cm^{-1} of the free benzaldehyde (see Fig. S9). This experiment demonstrated the possible activation of the substrate by the Sm^{3+} cations as Lewis acid site in **1** and **3**. Furthermore, the control experiment for cyanosilylation of benzaldehyde with $(NH_4)_6[Co_2Mo_{10}H_4O_{38}]\cdot 7H_2O$ precursor in a homogeneous manner gave 59.9% yield, which is far lower than that of **1** and **3** in the heterogeneous manner. The higher yield with **1** and **3** is possibly attributed to the synergistic effect of

the Lewis acid (Sm^{3+} cations) and the Lewis base (surface oxygen atoms of the $[Co_2Mo_{10}H_4O_{38}]^{6-}$ POM) that activate respectively aldehydes and TMSCN at the same time.

Conclusions

In summary, we have reported two racemic compounds (**1**, **2**) and two chiral conglomerates (**3**, **4)** in the reaction system of Evans-Showell type polyoxoanion $[Co_2Mo_{10}H_4O_{38}]^{6-}$ and lanthanide cations by changing the temperatures. The reaction temperature playing a crucial role to mediate the formation of racemic species vs conglomerates in the field of POMs, is for the first time demonstrated. Furthermore, these new POM materials containing lanthanides are efficient heterogeneous Lewis acid−base catalysts for cyanosilylation of various aldehyde compounds under solvent-free conditions. The successful isolation of these species not only certainly provokes researchers' interest to develop new catalytic materials containing POMs and lanthanides, but also provides incentives for more studies to spontaneous resolution of chiral POMs by controlling the reaction temperatures.

Supplementary information

The coordination modes of Sm^{3+} cations in **1** and **3**, 3D supramolecular topology structure for **3**, IR, TG curves and PXRD patterns for **1**–**4**, PXRD and IR figures after catalysis and before catalysis for **1** and **3** are available. Study on recycling of catalysts **1** and **3** are listed in Table S2.

Acknowledgement

The authors thank the National Natural Science Foundation of China (21371027, 20901013) and Fundamental Research Funds for the Central Universities (DUT12LK01) for financial supports.

References

1 (*a*) V. Soghomonian, Q. Chen, R. C. Haushalter, J. Zubieta and C. J. O'Connor, *Science*, 1993, **259**, 1596; (*b*) D. Y. Du, L. K. Yan, Z. M. Su, S. L. Li Y. Q. Lan and E. B. Wang, *Coord. Chem. Rev.*, 2013, **257**, 702; (*c*) X. X. Zheng, L. Zhang, J. Y. Li, S. Z. Luo and J. P. Cheng, *Chem. Commun.*, 2011, **47**, 12325.

2 (*a*) F. B. Xin and M. T. Pope, *J. Am. Chem. Soc.*, 1996, **118**, 7731; (*b*) M. Sadakane, M. H. Dickman and M. T. Pope, *Inorg. Chem.*, 2001, **40**, 2715; (*c*) M. Inoue and T. Yamase, *Bull. Chem. Soc. Jpn.*, 1995, **68**, 3055; (*d*) X. K. Fang, T. M. Anderson and C. L. Hill, *Angew. Chem. Int. Ed.*, 2005, **44**, 3540.

3 (*a*) U. Kortz, M. G. Savelieff, F. Y. A. Ghali, L. M. Khalil, S. A. Maalouf and D. I. Sinno, *Angew. Chem. Int. Ed.*, 2002, **41**, 4070; (*b*) C. Streb, D. L. Long and L. Cronin, *Chem. Commun.*, 2007, 471.

4 (*a*) H.Y. An, E. B. Wang, D. R. Xiao, Y. G. Li, Z. M. Su and L. Xu, *Angew. Chem. Int. Ed.*, 2006, **45**, 904; (*b*) H. Q. Tan, Y. G. Li, Z. M. Zhang, C. Qin, X. L. Wang, E. B. Wang and Z. M. Su, *J. Am. Chem. Soc.*, 2007, **129**, 10066.

5 (*a*) Y. Q. Lan, S. L. Li, Z. M. Su, K. Z. Shao, J. F. Ma, X. L. Wang and E. B. Wang, *Chem. Commun.*, 2008, 58; (*b*) L. Xu, C. Qin, X. L. Wang, Y. G. Wei and E. B. Wang, *Inorg. Chem.*, 2003, **42**, 7342.

6 B. Hasenknopf, K. Micoine, E. Lacôte, S. Thorimbert, M. Malacria and R.

Thouvenot, *Eur. J. Inorg. Chem.*, 2008, 5001.

7 (*a*) X. K. Fang, T. M. Anderson, Y. Hou and C. L. Hill, *Chem. Commun.*, 2005, **40**, 5044; (*b*) J. D. Compain, P. Mialane, A. Dolbecq, J. Marrot, A. Proust, K. Nakatani, P. Yu and F. Sécheresse, *Inorg. Chem.*, 2009, **48**, 6222.

8 (*a*) W. W. Ju, H. T. Zhang, X. Xu, Y. Zhang and Y. Xu, *Inorg. Chem.*, 2014, **53**, 3269; (*b*) H. Naruke, J. Iijima and T. Sanji, *Inorg. Chem.*, 2011, **50**, 7535; (*c*) Q. X. Han, C. He, M. Zhao, B. Qi, J. Y. Niu and C. Y. Duan, *J. Am. Chem. Soc.*, 2013, **135**, 10186; (*d*) Z. M. Zhang, Y. G. Li, S. Yao, E. B. Wang, Y. H. Wang and R. Clérac, *Angew. Chem. Int. Ed.*, 2009, **48**, 1581; (*e*) Z. M. Zhang, S. Yao, Y. G. Li, R. Clérac, Y. Lu, Z. M. Su and E. B. Wang, *J. Am. Chem. Soc.*, 2009, **131**, 14600.

9 (*a*) Y. Z. Wang, H. L. Li, C. Wu, Y. Yang, L. Shi and L. X. Wu, *Angew. Chem. Int. Ed.*, 2013, **52**, 4577; (*b*) T. Noguchiab and N. Kimizuka, *Chem. Commun.*, 2014, **50**, 599.

10 (*a*) Q. Tang, S. X. Liu, Y. W. Liu, S. J. Li, F. J. Ma, J. X. Li, S. T. Wang and C. Z. Liu, *Dalton Trans.*, 2013, **42**, 8512; (*b*) Y. Wang, S. L. Pan, H. W. Yu, X. Su, M. Zhang, F. F. Zhang and J. Han, *Chem. Commun.*, 2013, **49**, 306; (*c*) M. Sarma, T. Chatterjee, H. Vindhya and S. K. Das, *Dalton Trans.*, 2012, **41**, 1862; (*d*) J. Iijima, E. Ishikawa, Y. Nakamuraa and H. Naruke, *Inorg. Chim. Acta*, 2010, **363**, 1500; (*e*) Y. Wang, L. M. Wang, Z. F. Li, Y. Y. Hu, G. H. Li, L. N. Xiao, T. G. Wang, D. F. Zheng, X. B. Cui and J. Q. Xu, *CrystEngComm*, 2013, **15**, 285.

11 (*a*) I. Katsuki, Y. Motoda, Y. Sunatsuki, N. Matsumoto, T. Nakashima and M. Kojima, *J. Am. Chem. Soc.*, 2002, **124**, 629; (*b*) C. P. Brock, W. B. Schweizer and J.

D. Dunitz, *J. Am. Chem. Soc.*, 1991, **113**, 9811; (*c*) Y. Ma, Z. B. Han, Y. K. He and L. G. Yang, *Chem. Commun.*, 2007, 4107.

12 Y. Hou, X. K. Fang and C. L. Hill, *Chem. Eur. J.*, 2007, **13**, 9442.

13 (*a*) J. Zhang, J. Hao, Y. G. Wei, F. P. Xiao, P. C. Yin and L. S. Wang, *J. Am. Chem. Soc.*, 2010, **132**, 14; (*b*) F. P. Xiao, J. Hao, J. Zhang, C. L. Lv, P. C. Yin, L. S. Wang and Y. G. Wei, *J. Am. Chem. Soc.*, 2010, **132**, 5956.

14 (*a*) H. Q. Tan, Y. G. Li, W. L. Chen, D. Liu, Z. M. Su, Y. Lu and E. B. Wang, *Chem. Eur. J.*, 2009, **15**, 10940; (*b*) H. Q. Tan, Y. G. Li, W. L. Chen, A. X. Yan, D. Liu and E. B. Wang, *Cryst. Growth Des.*, 2012, **12**, 1111.

15 H. T. Evans and J. S. Showell, *J. Am. Chem. Soc.*, 1969, **91**, 6881.

16 (*a*) X. L. Wang, D. Zhao, A. X. Tian and J. Ying, *CrystEngComm*, 2013, **15**, 4516; (*b*) H. Y. Liu, H. Wu, J. Yang, Y. Y. Liu, B. Liu, Y. Y. Liu, and J. F. Ma, *Cryst. Growth Des.*, 2011, **11**, 2920.

17 (*a*) J. Q. Sha, J. Peng, Y. Q. Lan, Z. M. Su, H. J. Pang, A. X. Tian, P. P. Zhang and M. Zhu, *Inorg. Chem.*, 2008, **47**, 5145; (*b*) G. G. Gao, C. Y. Song, X. M. Zong, D. F. Chai, H. Liu, Y. L. Zou, J. X. Liu and Y. F. Qiu, *CrystEngComm*, 2014, **16**, 5150.

18 (*a*) K. Suzuki, M. Shinoe and N. Mizuno, *Inorg Chem.*, 2012, **5**, 11574; (*b*) F. Yu, X. J. Kong, Y. Y. Zheng, Y. P. Ren, L. S. Long, R. B. Huang and L. S. Zheng, *Dalton Trans.*, 2009, 9503; (*c*) H. Y. Zhao, J. W. Zhao, B. F. Yang, H. He and G. Y. Yang, *CrystEngComm*, 2013, **15**, 8186.

19 J. Y. Niu, J. A. Hua, X. Ma and J. P. Wang, *CrystEngComm*, 2012, **14**, 406.

20 S. G. Mitchell, T. Boyd, H. N. Miras, D. L. Long and L. Cronin, *Inorg. Chem.*, 2011, **50**, 136.

21 R. Dessapt, D. Kervern, M. Bujoli-Doeuff, P. Deniard, M. Evain and S. Jobic, *Inorg. Chem.*, 2010, **49**, 11309.

22 (*a*) G. A. Tsigdinos, Ph.D. Thesis, Boston University, 1961; (*b*) A. L. Nolan, R. C. Burns and G. A. Lawrance, *Dalton Trans.*, 1996, 2629; (*c*) U. Lee and H. C. Joo, *Acta Cryst.*, 2010, **E66**, i10.

23 (*a*) G. M. Sheldrick, SHELXL 97, Program for Crystal Structure Refinement, University of Gőttingen, Germany, 1997; (*b*) G. M. Sheldrick, SHELXL 97, Program for Crystal Structure Solution, University of Gőttingen, Germany, 1997.

24 J. Moreau, O. Delpoux, E. Devers, M. Digne and S. Loridant, *J. Phys. Chem. A*, 2012, **116**, 263.

25 C. Friedheim and F. Keller, *Ber.*, 1906, **39**, 4301.

26 I. D. Brown and D. Altermatt, *Acta. Crystallogr., Sect. B*, 1985, **41**, 244.

27 C. I. Cabello, F. M. Cabrerizo, A. Alvarez and H. J. Thomas, *J. Mol. Catal. A*, 2002, **186**, 89.

28 (*a*) K. Suzuki, M. Sugawa, Y. Kikukawa, K. Kamata, K. Yamaguchi and N. Mizuno, *Inorg. Chem.*, 2012, **51**, 6953; (*b*) R. F. D'Vries, M. Iglesias, N. Snejko, E. Gutiérrez-Puebla and M. A. Monge, *Inorg. Chem.*, 2012, **51**, 11349.

29 (*a*) Q. X. Han, X. P. Sun, J. Li, P. T. Ma and J. Y. Niu, *Inorg. Chem.*, 2014, **53**, 6107; (*b*) Y. J. Kikukawa, K. Suzuki, M. Sugawa, T. Hirano, K. Kamata, K. Yamaguchi and N. Mizuno, *Angew. Chem. Int. Ed.*, 2012, **51**, 3686.

30 R. F. D'Vries, V. A. Peña-O'Shea, N. Snejko, M. Iglesias, E. Gutiérrez-Puebla and M. A. Monge, *Cryst. Growth Des.*, 2012, 1**2**, 5535.

Table 1 Crystal data and structure refinement for **1**–**4**.

Complex	**1**	**2**	**3**	**4**
formula	$H_{40}Co_2Mo_{10}O_{56}Sm_2$	$H_{40}Co_2Mo_{10}O_{56}Eu_2$	$H_{40}Co_2Mo_{10}N_3O_{50}Sm$	$H_{40}Co_2Mo_{10}N_3O_{50}Eu$
formula weight	2314.28	2317.50	2109.96	2111.57
T (K)	293(2)	296(2)	296(2)	296(2)
crystal system	Triclinic	Triclinic	Monoclinic	Monoclinic
space group	*P*-1	*P*-1	*P*2(1)	*P*2(1)
a (Å)	12.458(3)	12.360(4)	10.5118(5)	10.5122(5)
b (Å)	13.915(3)	13.803(4)	18.6632(8)	18.6663(9)
c (Å)	14.341(3)	14.183(4)	12.2190(6)	12.2157(6)
α (˚)	74.555(3)	74.436(5)	90	90
β (˚)	85.531(3)	85.442(5)	114.115(2)	114.060(2)
γ (˚)	89.871(2)	89.734(5)	90	90
U (Å^3)	2388.5(9)	2323.2(12)	2187.96(18)	2188.76(18)
Z	2	2	2	2
μ (mm^{-1})	5.750	6.084	4.948	5.037
Flack parameters			0.025(8)	0.042(8)
reflections collected	13309	11088	9942	8771
independent reflections	8270	7967	9942	8771
R(int)	0.0319	0.0581	0.0000	0.0000
GOF on F^2	1.024	1.071	1.046	1.054
$R_1{}^a$ [I >2σ(I)]	0.0384	0.0976	0.0280	0.0301
$wR_2{}^b$[I >2σ(I)]	0.0981	0.2265	0.0743	0.0812
R_1 (all data)	0.0478	0.1362	0.0283	0.0302
wR_2 (all data)	0.1039	0.2493	0.0745	0.0813

$^aR1 = \sum||F_0|-|F_C||/\sum|F_0|$; $^bwR2 = \sum[w(F_0^2-F_C^2)^2]/\sum[w(F_0^2)^2]^{1/2}$

Table 2 Cyanosilylation of aldehydes catalyzed by compounds **1**–**4**[a].

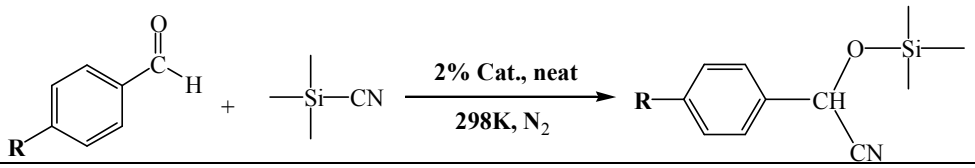

Compound	Aldehyde	Time (h)	Yield (%)[b]
1	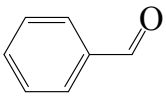	5	98.2
2		5	98.1
3		5	98.4
4		5	98.0
1	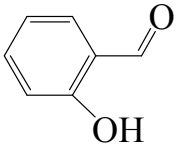	2	98.4
3		2	98.0
1	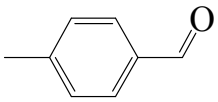	3	96.5
3		3	97.9
1	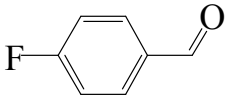	4	97.3
3		4	90.1
1	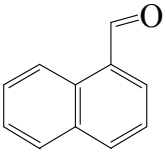	5	61.5
3		5	80.1
Blank	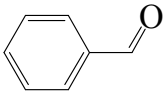	5	13.7
$(NH_4)_6[Co_2Mo_{10}H_4O_{38}]$	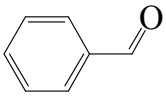	5	59.9

[a]Reaction conditions: catalyst 2 mol%, aldehyde 0.5 mmol, TMSCN 1.5 mmol, without solvent, room temperature (25°C) under N_2.

[b]Yields were determined by GC analysis using naphthalene as an internal standard.

Figure Captions

Fig. 1 (a) ORTEP drawing of **1** with thermal ellipsoids at 50% probability. Free water molecules are omitted for clarity. (b) ORTEP drawing of **3** with thermal ellipsoids at 50% probability. Free water molecules and ammonia ions are omitted for clarity.

Fig. 2 (a) In compound **1**, the homochiral polyoxoanions $[Co_2Mo_{10}H_4O_{38}]^{6-}$ are respectively connected by Sm^{3+} to a left-handed chain and a right-handed chain. (b) Polyhedral representation of 1D non-chiral ladder in **1**, showing the left-handed and right-handed chiral chains linked by Sm^{3+} cations.

Fig. 3 (a) 2D supramolecular layer in **1**, showing the strong hydrogen bonds between polyoxoanions and coordinated water molecules with blue colour. (b) A view along the *b* axis illustrating the 3D supramolecular framework displaying the interbedded hydrogen bonds with yellow colour in **1** (color code: Co, yellow; Mo, pink/blue; Sm, green; O, red). Free water molecules are omitted for clarity.

Fig. 4 (a) Polyhedron and ball-stick view of the 1D supramolecular chiral chain in **3** through the hydrogen-bonding interactions between the terminal oxygen atoms of polyoxoanions and coordinating water molecules. (b) View of 2D supramolecular chiral sheet in **3** showing the hydrogen-bonding interactions between polyoxoanions and coordinating water molecules, (color code: Co, yellow; Mo, blue; Sm, green; O, red; hydrogen bond, green).

Fig. 5 View of the 3D supramolecular chiral framework of **3** along the *c* axis, (color code: Co, yellow; Mo, blue; Sm, green; O, red; hydrogen bond, green or yellow).

Fig. 6 (a) UV−vis diffuse reflectance spectra of bulk compounds **1** and **2**. (b) UV−vis

diffuse reflectance spectra of bulk compounds **3** and **4**.

Fig. 7 The solid state CD spectra of the crystalline powders L-**3** and D-**3**, respectively showing the opposite Cotton effects.

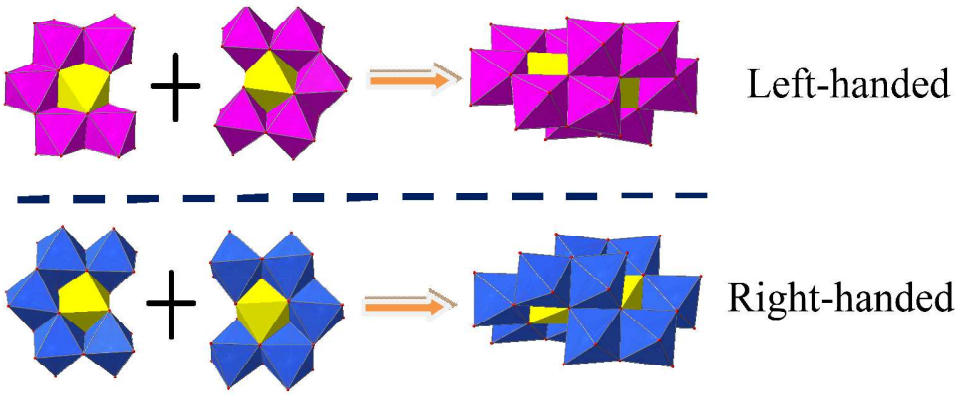

Scheme 1 L-$[Co_2Mo_{10}H_4O_{38}]^{6-}$ and D-$[Co_2Mo_{10}H_4O_{38}]^{6-}$ with D_2 symmetry viewed as two "parent clusters" $\{CoMo_5O_{19}\}$ turning one ~45° around the anionic equatorial plane and joining together by sharing an edge.

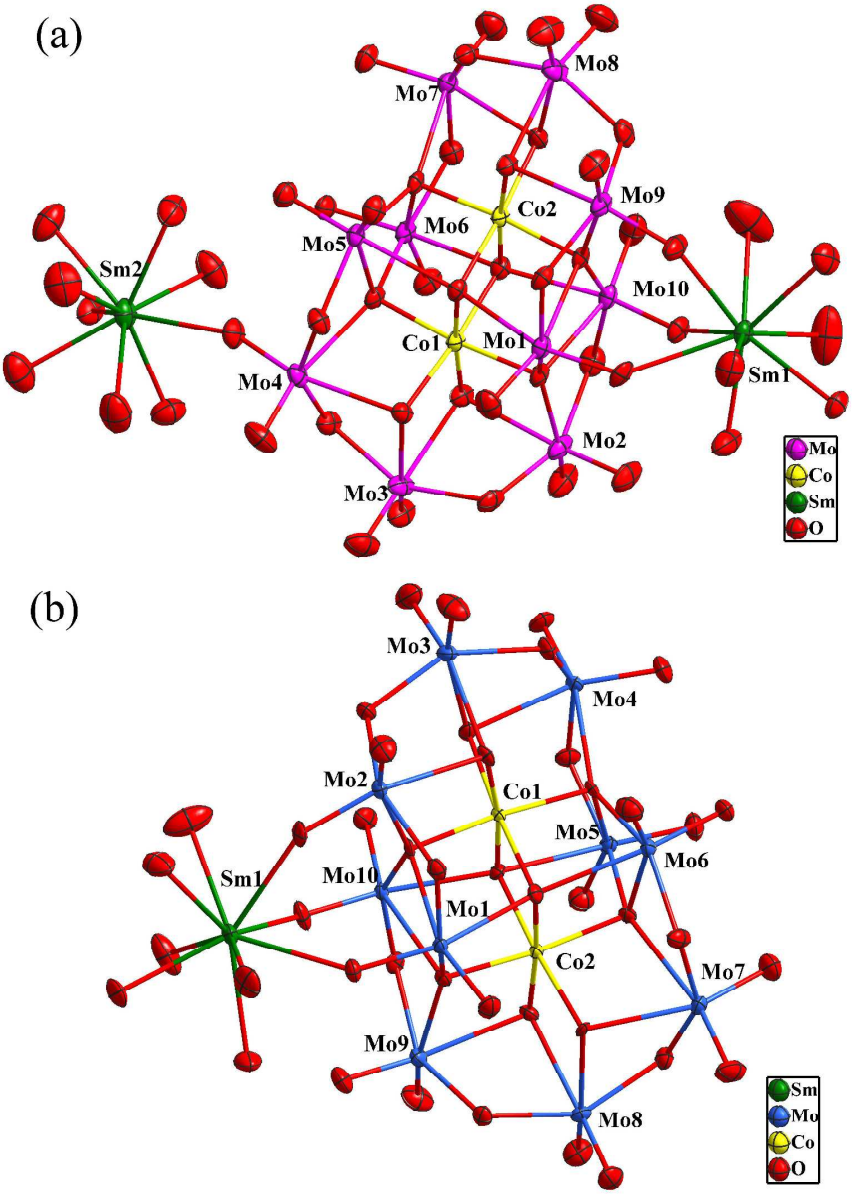
(a)
Mo8
Mo7
Co2
Mo9
Mo6
Mo5
Sm2
Mo10
Co1
Mo1
Sm1
Mo4
Mo2
Mo3
Mo
Co
Sm
O
(b)
Mo3
Mo4
Mo2
Co1
Mo5
Mo6
Sm1
Mo10
Mo1
Co2
Mo7
Mo9
Mo8
Sm
Mo
Co
O

Fig. 1

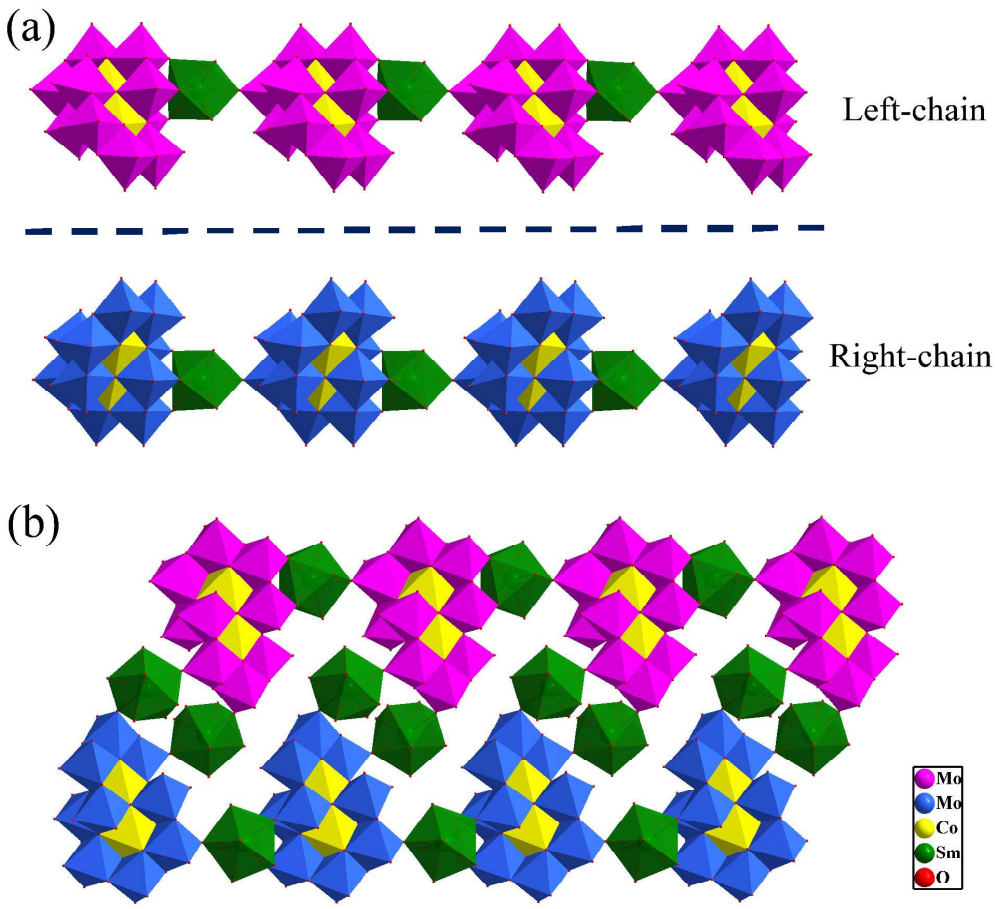

Fig. 2

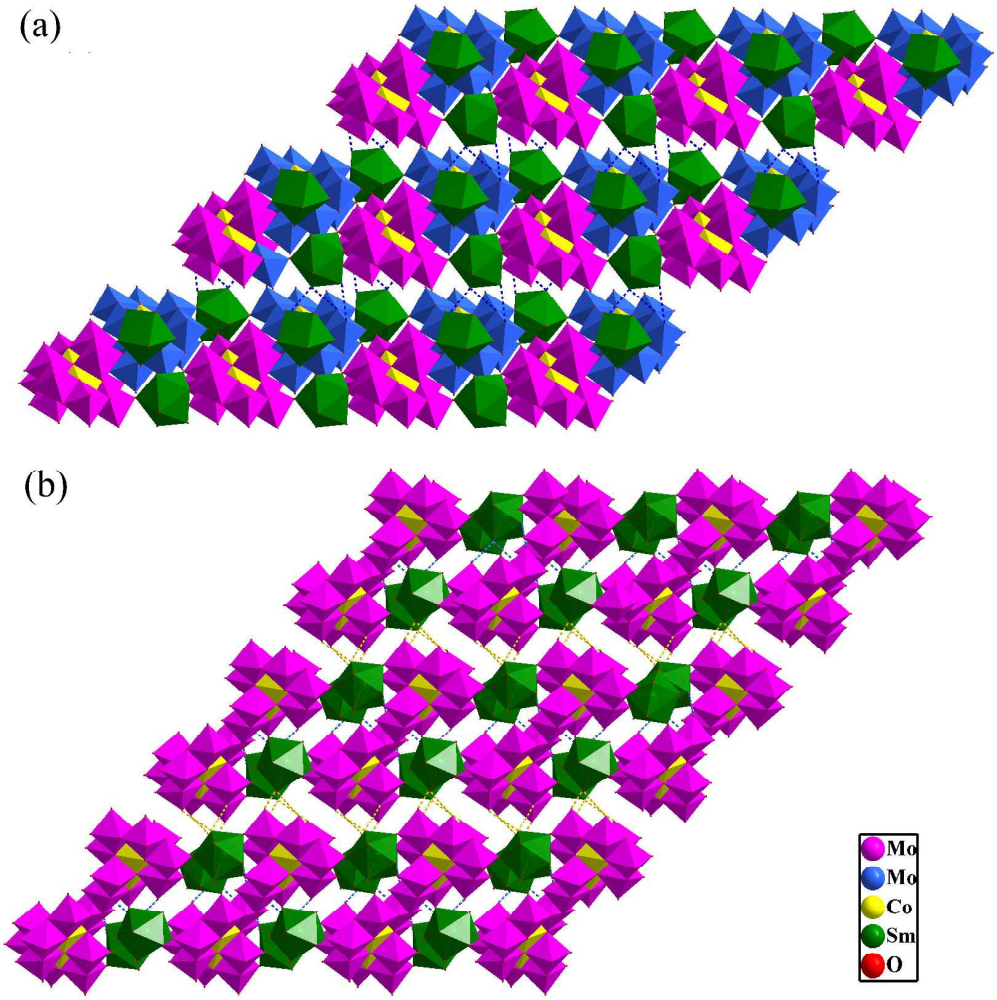

Fig. 3

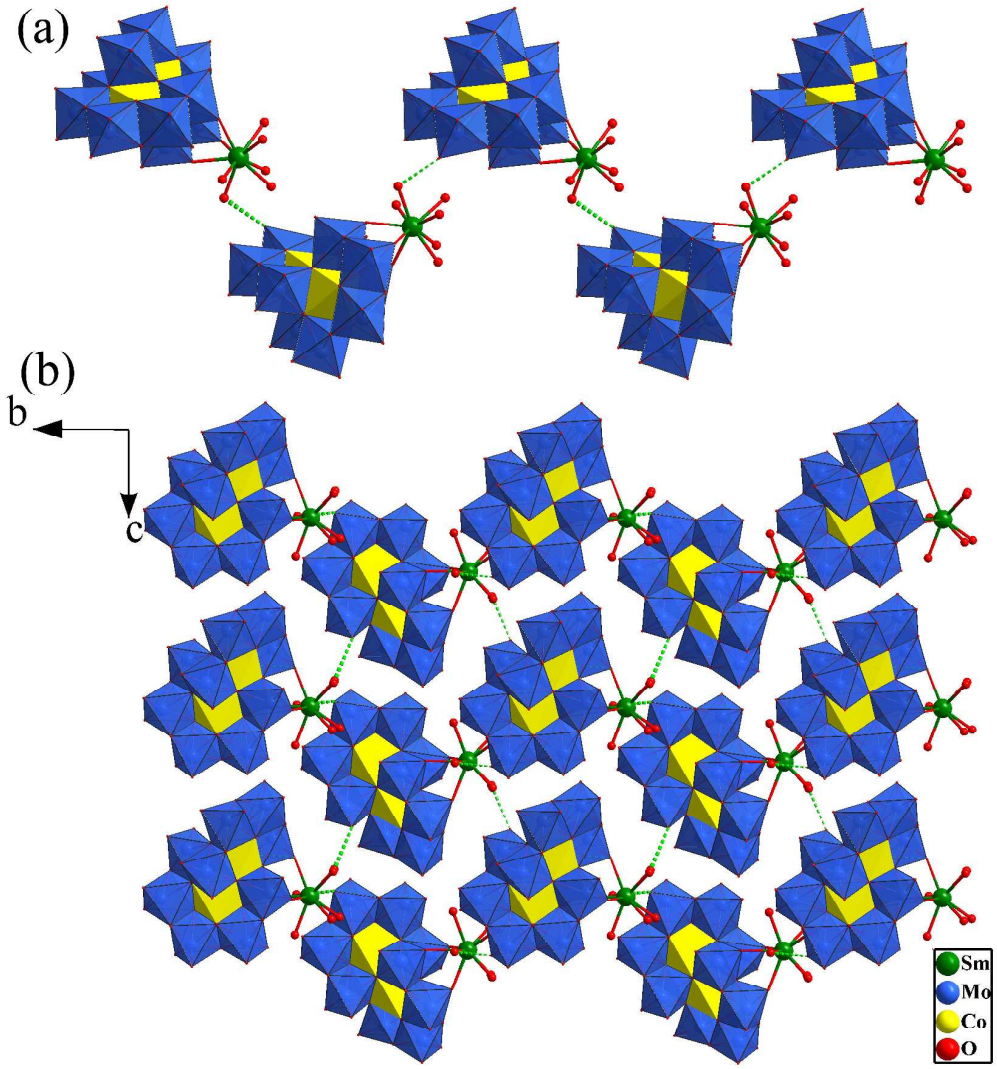

Fig. 4

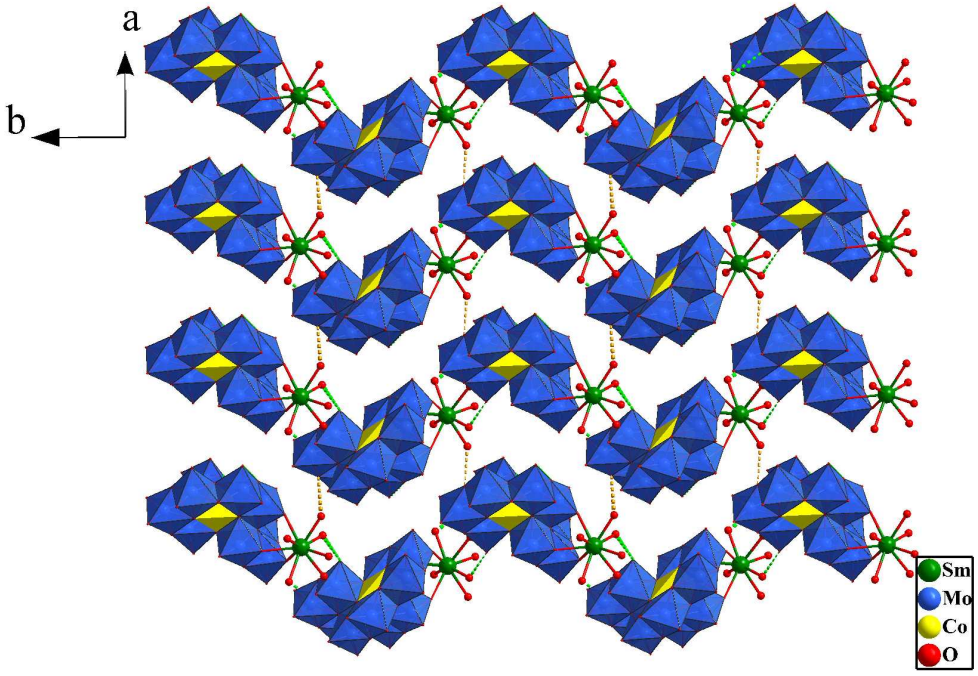

Fig. 5

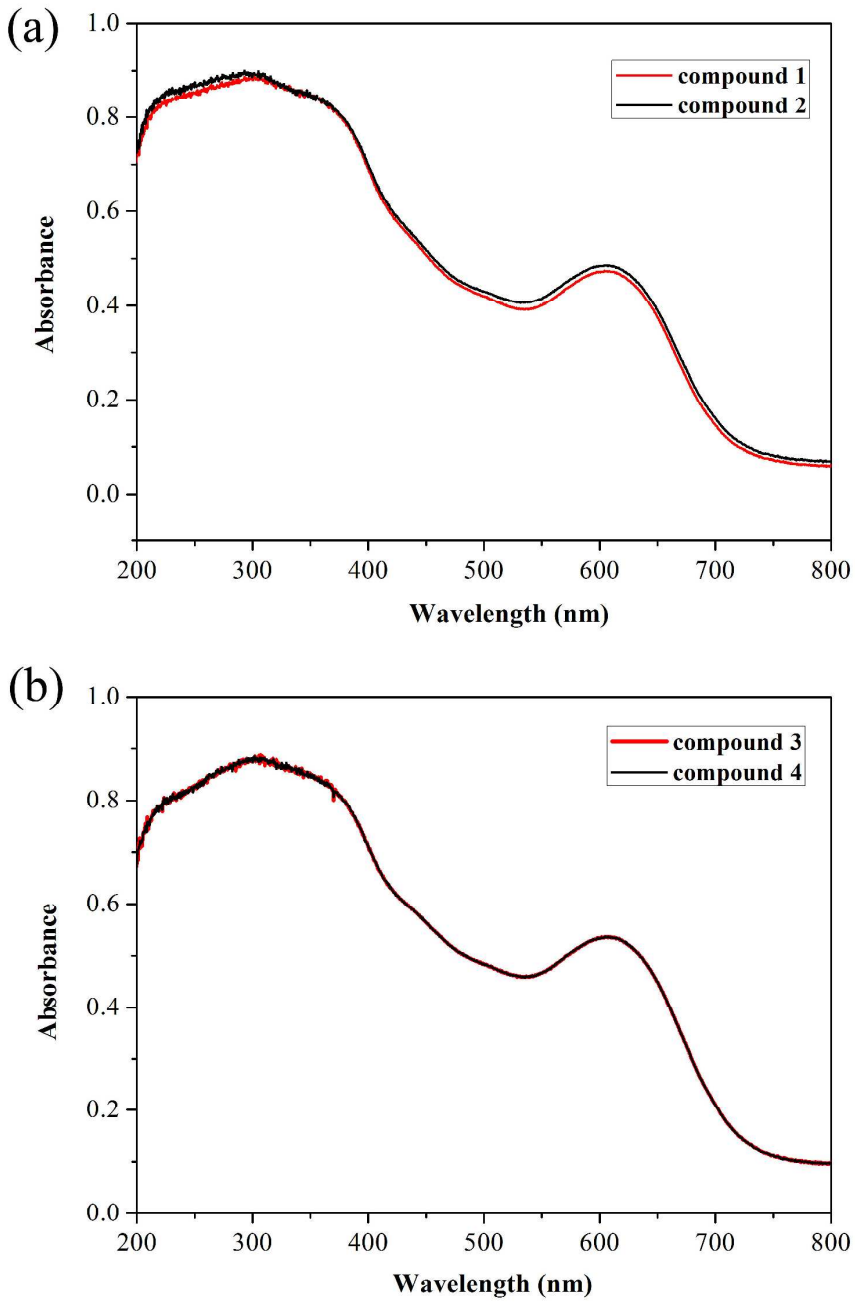
(a)
Absorbance
Wavelength (nm)
compound 1
compound 2
(b)
Absorbance
Wavelength (nm)
compound 3
compound 4

Fig. 6

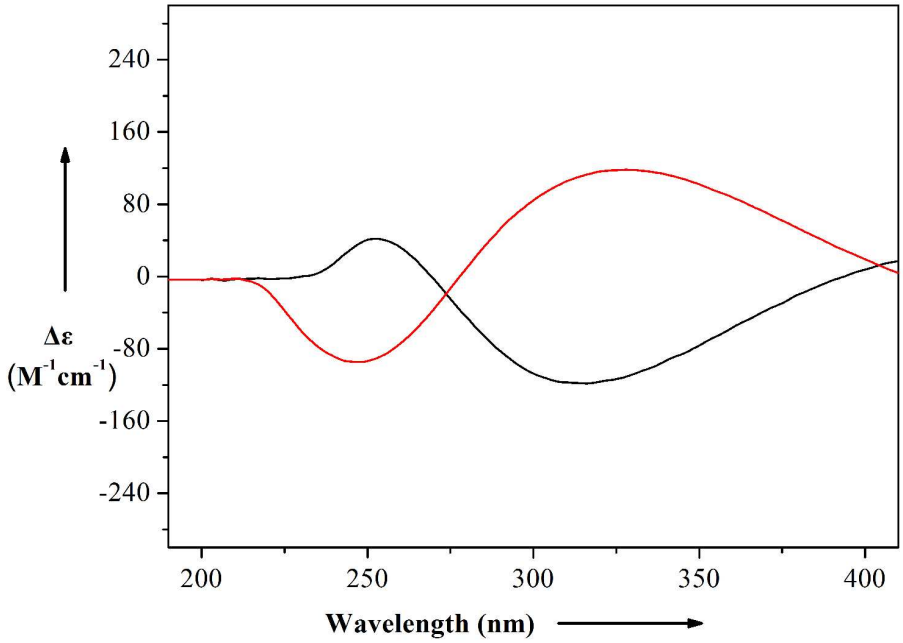
240
160
80
0
-80
-160
-240
Δε
(M-1cm-1)
200
250
300
350
400
Wavelength (nm)

Fig. 7

Table of Contents

Temperature-induced racemic compounds and chiral conglomerates based on polyoxometalates and lanthanides: syntheses, structures and catalytic properties

Haiyan An,* Lin Wang, Ying Hu, Fei Fei

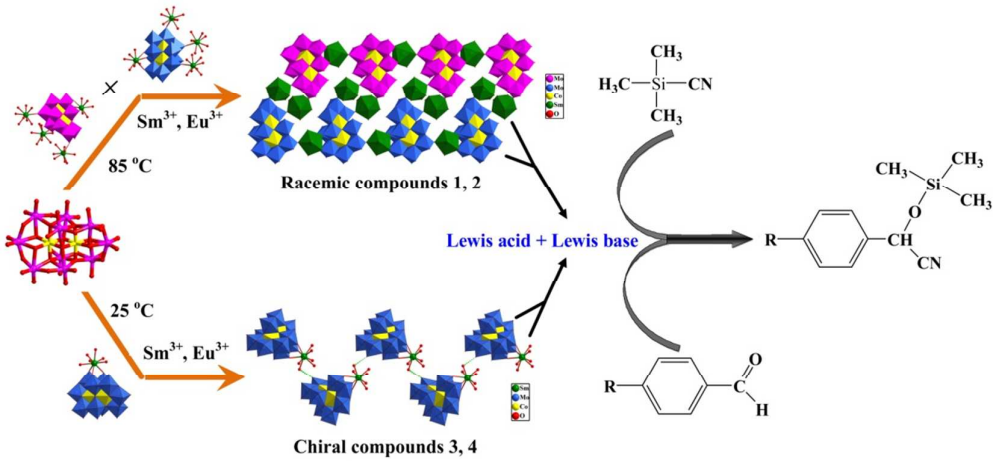

Four new species, originated from $[Co_2Mo_{10}H_4O_{38}]^{6-}$ and lanthanides by adjusting reaction temperatures, are reported, which act as Lewis acid-base catalysts toward the cyanosilylation reaction.